# *CHAPTER 3*

## *SYNTHESIS, STRUCTURAL AND MAGNETIC ANALYSIS OF $CoFe_2O_4$:$SiO_2$ NANOCOMPOSITES*

### 3.1 Introduction

In this chapter preparation, synthesis of $CoFe_2O_4$: $SiO_2$ nanocomposites have been carried out by the coprecipitation technique. The $CoFe_2O_4$: $SiO_2$ nanocomposites are further investigated by various characterization techniques to analyze and study their important parameters. Here a brief introduction is presented. Nanostructure materials because of their small size, correspondingly high surface to volume ratio and quantum confinement effect have attracted considerable attention as comparatively their bulk materials [1, 2]. Ferrites are one of the most dealt nanostructured materials due to the exclusive and exceptional features possessed by them. Ferrite materials are insulating magnetic materials that possess better electrical resistivity, small eddy current and less dielectric losses, good saturation magnetization, high value of permeability and medium value of permittivity. No other material with such wide ranging of striking properties exists and therefore ferrites are exceptional magnetic materials with matchless features that own applications in almost all the fields. Properties of ferrites are highly responsive to preparation method, annealing conditions, quantity of constituents taken, doping and substitution. Therefore, the choice of an appropriate method is the way to achieve high quality ferrites [3-5]. Nanocrystalline ferrites originate many applications in a class of advanced fields thus extended their area of applications to a great extent [6-9]. Ferrites display dielectric properties. Revealing dielectric behaviour means that even after the passage of electromagnetic waves through them, ferrites do not conduct electricity. This wins an advantage for ferrites over other transition metals that conduct electricity. Another important feature that discriminates ferrites from others is the porosity, which possessed by ferrites and is completely irrelevant in metals. These are some mentioned reason that explain the importance of ferrites and show the motive of extensive research and study of ferrites being paid so much attention. The characteristics of ferrites are being enhanced due to the increasing demand of ferrites to meet the escalating trends in technology. Ferrites technology has obviously a bright future [10]. Basically ferrites are classified as spinel, garnet and magneto-plumbite types. All of these ferrites have their own unique identity

and show different important applications. Magneto-plumbite ferrites represented by formula $MFe_{12}O_{19}$, where M= Sr, Ba, Ca etc and are useful in permanent magnetic applications. Garnets are represented by the formula $Me_3Fe_5O_{12}$ where Me stands for rare earth ions or Yttrium and usually have relevance in microwave system applications. Spinel ferrites display chemical formula $MFe_2O_4$ where M is divalent cations such as Co, Zn, Ni, Cd. Spinel possess cubic close packed structure of oxygen and ions. The crystal of spinel ferrite mainly comprises of two interstitial sites that are tetrahedral (A) and octahedral [B] sites which hold the distribution of cations with different ionic [11]. Among ferrites, the spinel ferrites are highly attractive magnetic nanoparticles because of their many uses in various fields together with permanent magnets, ferro-fluid technology, medical diagnostics, magnetic type drug delivery, microwave frequency devices, catalysis and high density information data storage [12-18]. The general representation of the spinel-type ferrites may be written as $(A_{(1x)}B_x)_{tet}$ $[A_xB_{(2-x)}]_{oct}O_4$, The notions *x, tet* and *oct* stands for degree of inversion / disorder parameter, tetrahedral and octahedral. For *x* value 0, the cations are orderly placed onto the two cationic sites and structural formula modifies to $(A)_{tet}[B_2]_{oct}O_4$, and the spinels show the normal cationic behaviour. The opposite to normal spinels are inverse spinels that come into picture at *x* value 1, formula analogous to $(B)_{tet}[AB]_{oct}O_4$ [19]. Again in these spinel ferrites, the cobalt ferrite ($CoFe_2O_4$) has been of great importance in fundamental science and technology due to their exceptional magnetic properties like large value of coercivity (Hc), moderate value of saturation magnetization (Ms), high magnitude of mechanical hardness and good chemical- stability [20]. As, cobalt ferrite shows inverse spinel behaviour represented by $(Co_{1-x}\ Fe_x)$ A $(Co_xFe_{2-x})$ $BO_4$, here x indicates degree of inversion, while A and B corresponds to tetragonal and octahedral sites respectively. The characteristics of $CoFe_2O_4$ vary as per the source it is obtained from such as bulk or nanoparticles. Literature survey [21-25] reveals the variation in magnetic properties with particle size. For example, at room temperature, the values of saturation magnetization and coercivity were recorded. For a change in particle size from 4 nm to 50 nm, a change of 30 to 80 emu g-1 for saturation magnetization and a variation of 0.5 to 5.4 kOe in coercivity value were observed. Also thermal changes are dominating in tiny particles possessing low anisotropy [26-28]. However, cobalt ferrites are having very strong affinity to agglomerate; consequently it is very difficult to expose their distinctive physical behaviour needed for some important applications. To conquer this difficulty, nanoparticles are very well embedded in an insulating type

silica matrix which allows stabilization of the nanoparticles [29, 30]. Silica matrix controls the particle growth and thus stabilising particles and also matrix acts as a shielding from the external environment. This shield prevents the damage to nanoparticles. Now to disperse cobalt ferrite nanoparticles to silica matrix, there is a need of appropriate technique which could better reveal the properties of nanocomposites. Thus, synthesis of nanoparticles is an exciting and challenging area of research for their technological and biomedical applications. In this direction, many synthesis strategies have been employed for the preparation of nanosized spinel ferrites like ball milling, sono-chemical, sol-gel, chemical co-precipitation, hydrothermal etc [31-37]. This chapter deals with the structural and magnetic properties of nanocomposites of cobalt ferrite ($CoFe_2O_4$) dispersed in silica matrix. Coprecipitation technique is employed to fabricate silica dispersed cobalt ferrite ($CoFe_2O_4$: $SiO_2$) nanocomposites. Moreover, thermal analysis was also employed to study the thermal variations of nanocomposites as a function of annealing temperature.

### 3.2 Sample Synthesis and Characterization

Various nanocomposites samples of cobalt ferrites dispersed in silica ($CoFe_2O_4$:$SiO_2$) were prepared and synthesized with the help of co-precipitation technique as described below:

Preparation of $CoFe_2O_4$ suspension solution was carried out by using high purity precursors of nitrates: cobalt nitrate hexahydrate ($Co(NO_3)_2$ .$6H_2O$), ferric nitrate nonahydrate ($Fe(NO_3)_3.9H_2O$), ammonia hydroxide ($NH_4OH$). In this method $Co(NO_3)_2.6H_2O$ and $Fe(NO_3)_3.9H_2O$ were taken in the form of molar ratio 1:2 of [Co2+]/ [Fe3+] and then were dissolved in double distilled water and stirred briskly at 70 $^oC$ in different vessels. After a continuous and constant stirring for about 6 hrs, a uniform solution of both the salts was obtained. In the next step, the iron nitrate solution and cobalt nitrate solution were mixed together at a constant stirring rate of 300 r.p.m. The mixture solution of both the solvents was kept on stirring for next 6 hrs in order to obtain a uniform solution. In this work, double distilled water was used as a solvent in order to avoid impurities. Continuous stirring of blended iron precursors and cobalt precursors at 70 $^oC$ formed a brown coloured clear solution. Ammonia hydroxide was used as a base and added dropwise to the above obtained solution to monitor a pH value of 12 so as for obtainment of better precipitates from $CoFe_2O_4$ solution. Afterwards resultant

precipitated solution was washed down with double distilled water by many times to remove any impurities present within. Dark brown precipitates of $CoFe_2O_4$ in the form of suspension solution were obtained.

Next step was synthesis of $SiO_2$ solution. For that a typical molar ratio of TEOS: $C_2H_5OH$: $HNO_3$: $H_2O$: $NH_4OH$ precursors was taken as 1: 3: 0.01:1: 0.016 respectively.

All the above mentioned precursors in the $SiO_2$ synthesis step were stirred and mixed in the recommended ratio in double distilled water. During the mixing process, these precursors were kept on stirring constantly. After that ammonia hydroxide ($NH_4OH$) has been slowly added drop by drop in the TEOS, $C_2H_5OH$ and $HNO_3$ solution mixture. Addition of $NH_4OH$ turned the TEOS, $C_2H_5OH$ and $HNO_3$ solution mixture from transparent to milky. A milky suspension solution of silica was obtained. Further, this obtained suspension- solution was very well stirred constantly for 2 h at 60$^o$C.

In the third and final step, synthesis of $CoFe_2O_4$: $SiO_2$ nanocomposites was carried out by adding the suspension solution obtained in the first to the suspension solution obtained in step second followed by a continuous and constant stirring. The mixed suspension solution was stirred for 6 hours. This resulted in the formation of precipitates of $CoFe_2O_4$: $SiO_2$ in suspended form. Precipitates so obtained were filtered and washed with double distilled water to remove any impurity agent. The washed precipitates then placed carefully in a vacuum-oven at 80 $^o$C to get dry. The drying process lasted overnight. The dried precipitates obtained were further grinded in a pestal mortar to form a very fine-powder. Finally, this powder sample was further heat treated at 250$^o$C, 500$^o$C, 750$^o$C and 1000$^o$C in vacuum at a ramp rate of 4$^o$C/min using a programmable vacuum muffle furnace. After attaining the required temperature, samples were kept to rest for 2 hrs to cool down for the crystals to develop and settle down.

Measurements of XRD data was done by an X-ray diffractometer (Philips PW/1710) of mono-chromatic CuKα type radiation of wavelength1.548 Å (50KV, 40 mA). XRD pattern provides information regarding crystallite size, strain and lattice parameter. The FTIR spectra were recorded by using FTIR spectrometer (Perkin-Elmer 1600) to study information like phase transformation and bonding of

constituents in the frequency range 7800–350 $cm^{-1}$. Microstructure was analysed by scanning electron microscopy (SEM- JSM6610LV) with a maximum applied voltage of 30 kv. Surface morphology and microstructure of nanocrystallites was analysed by transmission electron microscopy (TEM-TECNAI 200kV) in vacuum with a maximum applied voltage 200kv. Measurements of magnetic properties of our prepared ferrites samples were performed at room temperature with the help of a vibrating sample magnetometer (VSM) Model ADE-EV9 under magnetic field limit of 2.2 Tesla. Variations in mass of samples as a function of temperature and decomposition of precursors is studied by TGA-DTG curve in temperature range of 25-1100 $^oC$ (FRS1 R-Type).

## 3.3 Results and their Discussion

### 3.3.1 X-ray Diffraction (XRD) Analysis

X-ray diffraction method is employed to study various structural parameters including miller indices, crystallite size, lattice parameter, stress/ strain, density, activation energy etc. In the present study, XRD patterns for $CoFe_2O_4$: $SiO_2$ nanocomposites defined as, as-prepared along with heat treated type at temperatures $250^0C$, $500^0C$ and $750^0C$ are analysed thoroughly. The analysis of different parameters of as-prepared and synthesized samples is elaborated section wise.

**Diffraction Planes and Miller Indices**

The diffraction planes for prepared samples were indexed by matching with a standard reference called JCPDS data. JCPDS data helps to identify and texting the planes that consists of a set of h, k, l indices. The miller indices of the diffractogram of prepared and synthesized samples were calculated by running check cell programme. Figure 3.1 represents the indexed X-ray patterns of $CoFe_2O_4$: $SiO_2$ nanocomposites.

From the diffractogram, it is revealed that planes at low temperature are not completely developed. Low temperature diffraction planes do not provide a complete set of information of diffraction planes. The proper knowledge and indexing of diffraction planes was made at comparatively higher temperature. Here the diffraction pattern annealed at 750 $^oC$ is indexed to denote diffraction planes. This XRD pattern of sample annealed at 750 $^oC$ presence of well developed intense peaks at $2\theta$ ~ $30.10^o$, $33.20^o$ (*), $35.57^o$, $43.16^o$, 54.10, $57.08^o$, $62.65^o$which could be attributed to cubic spinel structure with Fd3M phase group. The planes corresponding to indexed $2\theta$ values are (220),

(311), (400), (422), (511) and (440) diffraction planes and (*) is the characteristic peak referring to α- $Fe_2O_3$. The corresponding d values to these reflections are 2.96834, 2.69709, 2.52536, 2.09590, 1.69502, 1.61361, and 1.48284.

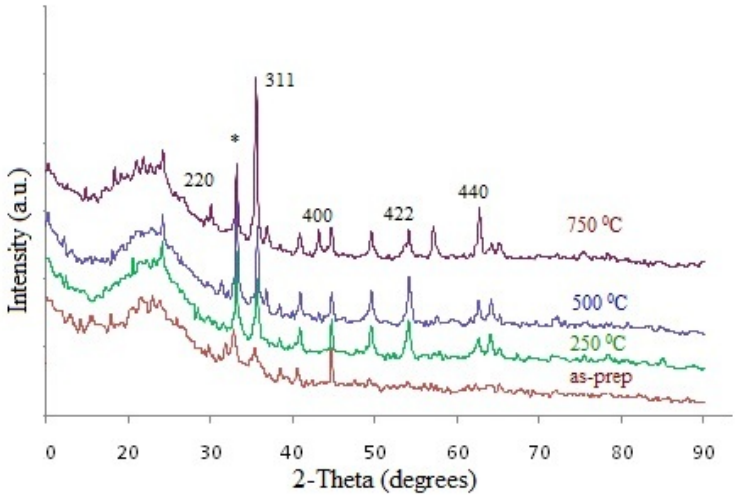


**Fig. 3.1: XRD patterns of as-prepared and thermally treated samples of $CoFe_2O_4$: $SiO_2$ nanocomposites**

**Lattice Parameter and Particle Size Description**

A very broad hump observed at 2θ around ~ 21-25$^o$ in these XRD traces for all the samples attribute to the amorphous $SiO_2$. The XRD pattern of as -prepared sample shows very faint peaks at 2θ around~ 35.05, 44.70, 55.72$^o$ which suggests almost no crystallinity of as -prepared sample. In order to study the effect of heat treatment on precursors, the as-prepared sample was annealed at low temperature~ at 250$^o$C for 2h. The XRD pattern of sample annealed at 250 $^o$C shows weak peaks indicating very poor crystallinity. In order to achieve the crystallinity of nanocomposites as-prepared sample was further heat treated at higher temperatures 500 $^o$C (2h) and 750 $^o$C (2h). As the temperature is further raised from 250 $^o$C to 500 $^o$C an observable difference in sharpness and intensity of peaks is noticed. This rise in temperature leads to some noticeable crystallinity of sample annealed at 500 $^o$C which could be clearly seen from figure 3.1. In the XRD patterns of sample heat treated from 250 $^o$C- 500 $^o$C two significant peaks are observed centred at 2θ~ 33.20$^o$ and 35.41$^o$. The peak at 2θ~ 30.10 $^o$C could be assigned characteristic peak of α- $Fe_2O_3$ [38] and peak centred at 2θ ~ 35.05$^o$C could be allocated as characteristic peak of $CoFe_2O_4$:$SiO_2$. The intensity of characteristic peak of α- $Fe_2O_3$ is found higher than that of characteristic peak of

$CoFe_2O_4$:$SiO_2$ indicates that ferrite phase is leading $CoFe_2O_4$: $SiO_2$phase in the temperature range of 250 $^oC$- 500 $^oC$. $CoFe_2O_4$ phase is not still completely developed. Literature reveals that ferrite silica composite has been mostly annealed in the temperature range 300- 700$^oC$. In order to study the effect of recrystallization temperature nearly that is 700 $^oC$ on ferrite: silica composite, we annealed the precursors at 750 $^oC$ for 2h.The recrystallization temperature is considered to around 0.8 times multiple of its melting temperature [39]. However, when the diffraction pattern was minutely examined, we noticed that intensity of peak centred at $2\theta \sim 35.57^o$ was increased while that of centred at $2\theta \sim 33.20^o$ is reduced. This sharp increase in the intensity of peak centred at $2\theta$ about $35.57^o$ indicates that $CoFe_2O_4$ particles are now nucleated in silica matrix. Evoking to spinel structures, which is further, divided into two standard structure types are normal spinel type and inverse spinel type. In normal spinels, distribution of divalent ions is solely on tetrahedral sites and distribution of trivalent is on octahedral sits. Inverse spinels have tetrahedral sites filled by half of trivalent and octahedral are occupied by other half of trivalent and full of divalent ions. At the nanolevel, the cationic distribution mixed type that is distribution is mid way of normal and inverse spinels [40]. The X-ray pattern generates when the incident light falls on a lattice plane and suffer reflection. These reflections correspond to Bragg's Law formulated as

$$\mathbf{2d_{hkl}\ Sin\theta_{hkl} = n\lambda} \qquad \mathbf{(3.1)}$$

Bragg's law presents relation between angle of propagation of scattered beam ( $\theta_{hkl}$) and inter planer spacing ($d_{hkl}$). Set 'hkl' represents miller indices and signifies property of material related to lattice constant [20, 41, 42]. $CoFe_2O_4$: $SiO_2$ being a cubic system follows the equation

$$\mathbf{d = \frac{a}{\sqrt{h^2+k^2+l^2}}} \qquad \mathbf{(3.2)}$$

The d spacing values and corresponding lattices planes are already mentioned above for the higher temperature of 750 $^oC$. By the knowledge of these two parameters, lattice constant/parameter (a) values are calculated and presented in table 3.1. The variations of lattice parameter noticed by increasing temperature could be attributed to ionic size of $Co^{2+}$ and $Fe^{3+}$ ions. As the temperature is raised, the cations tend to redistribute themselves on the preferred tetrahedral and octahedral locations. Divalent ions in their normal state prefer to occupy tetrahedral

locations being smaller than octahedral locations, but as they possess large ionic radii than those of trivalent ions that residing on octahedral sites, therefore without any size restriction, divalent can also move to octahedral locations or on the both locations. Basically, some cations (could be divalent or trivalent) instead of occupying their usual locations, moves to the interstitial positions. These cations are named as anti-site. The movements of cations on interstitial position is a consequence of method of preparation of and variations of parameters such as temperature, pressure etc. [43]. Variations with respect to thermal treatment of structural parameters of $CoFe_2O_4$: $SiO_2$ nanocomposites such as lattice parameter, grain size, microstrain and X-ray density have also been estimated. The change in lattice parameters as a function of temperature is also reported in the Fig. 3.2. Polynomial behaviour of lattice constant is observed with increasing annealing temperature. These increasing- decreasing variations of lattice parameters are mainly due to: (i) thermal effects, and (ii) re-equilibration of cations.

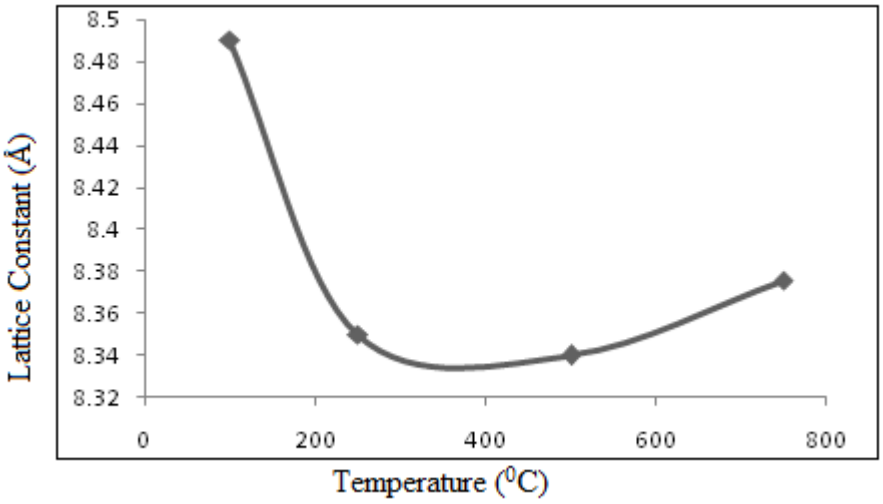


**Figure 3.2: Lattice constant versus annealing temperature**

The results of present investigation concludes that lattice constant decreases with increasing temperature up to 250°C and however, a sudden change in lattice constant with temperature is also observed which may be due to ordering-disordering transformation in the spinel. The variations in lattice constant as a function of temperature closely relate to phenomenon of re-equilibrate of cations. The movement of cations from one site to other or some interstitial position with temperature variation is an important factor that brings out the changes in cationic arrangement of spinels and this leads to transformation in characteristics also [44]. This process

is non- convergent as the structure and equilibrium remains unaltered. The grain size ($D_{D\text{-}S}$) of nanocomposites was also estimated by Debye-Scherrer equation (3.3) [45].

$$\beta = k\lambda/D_{D-S}\,Cos\theta \qquad (3.3)$$

The mean crystallite size of $CoFe_2O_4$: $SiO_2$ was estimated corresponding to the strongest reflection located about 35.57°. The values of crystallite size estimated from Debye- Scherrer equation are listed in table 3.1. Debye – Scherrer equation only deals with particle size purely, it does not cope with other factors originated in the lattice like stress, strain. As a matter of fact, it is a well known that the grain size and micro-strain produces peak broadening. This could be due to the stresses and faults inside the prepared spinel nanoparticles. The effects of grain size and strain are completely different and need to be distinguished. Although, these both type of effects are different from each other and can be discriminated. This may be understood with the help of size-strain plot. This plot for size-strain may also be known as Williamson-Hall plot (figure 3.3).

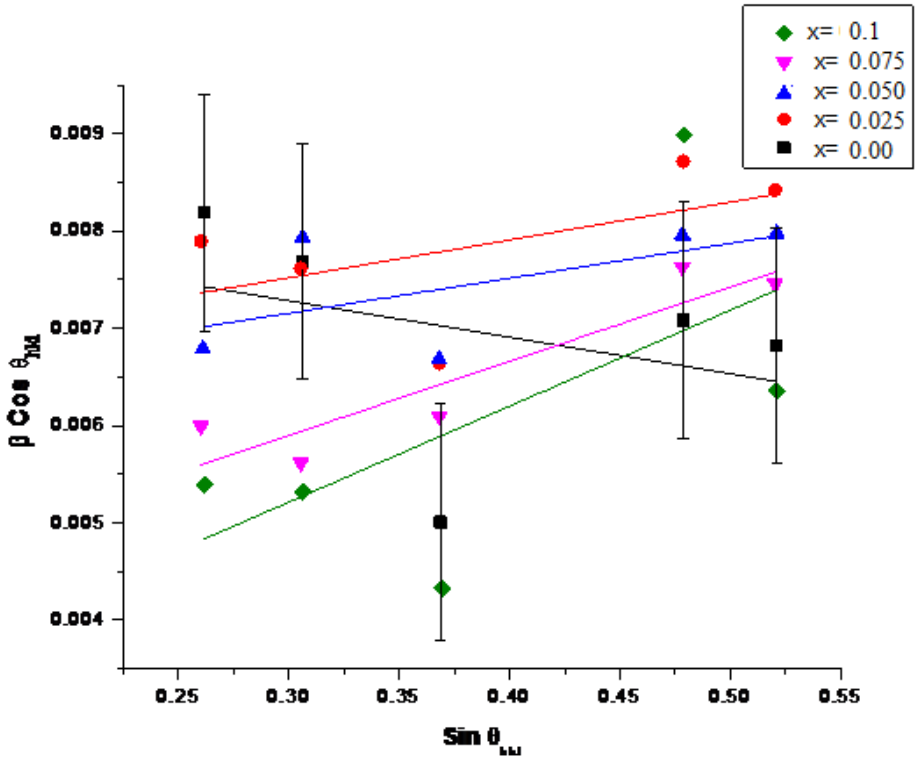


**Fig. 3.3: Williamson-Hall plot of as-prepared and annealed $CoFe_2O_4$: $SiO_2$ nanocomposites at different temperatures**

On the other hand, the particle size ($D_{W-H}$) was also calculated by considering the stress broadening with the use of Williamson- Hall method represented by equation 3.4

$$\beta = k\lambda / D_{W-H} \cos\theta + 4\varepsilon \sin\theta \qquad (3.4)$$

where ε represents coefficient of micro stress or strain. Micro-strain values have been obtained from slope of these fitted lines. The value of standard deviation corresponding to fitted lines estimated to be is 0.00121. The increase in particle size has been noticed from the Williamson-Hall plot as compared to Debye-Scherrer equation. This increase in size by Williamson-Hall plot method is due to the consideration of stress effects. By fitting the data, the average grain size ($D_{W-H}$) and micro-strain (ε) are estimated and given in the table 3.1.

The variations of particle size as a function of temperature is represented in figure 3.4. Almost a linear relationship is seen in between particle size and annealing temperature. Figure 3.4 represents Scott equation (3.5). Activation energy of nanoparticles is calculated from the Scott's equation.

$$D=C \exp(-E/RT) \qquad (3.5)$$

where D is mean crystallite size, E is activation energy, R is gas constant and T is annealing temperature.

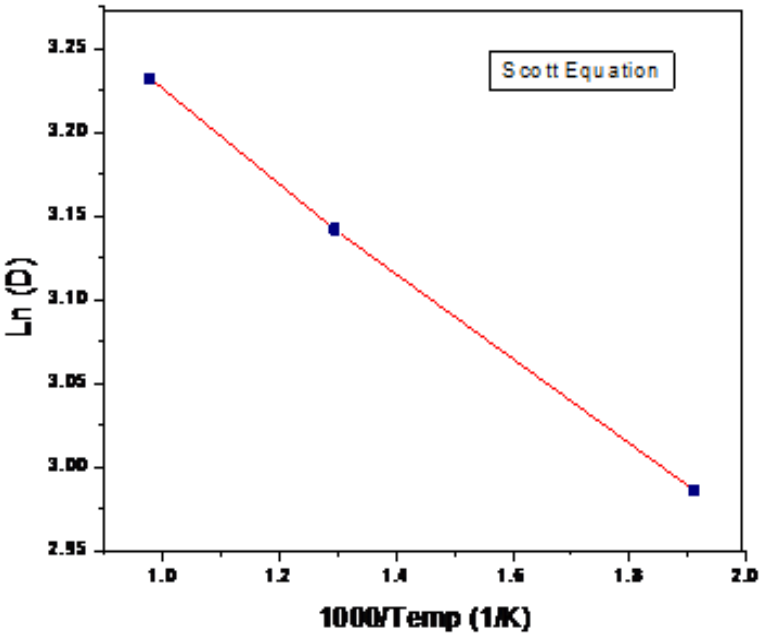


**Fig. 3.4: Crystallite size versus calcinations temperatures (Scott equation)**

The obtained value of activation energy is E= 0.22eV.

From the Table3.1, it could be seen that around the re-crystallization temperature, dislocations (micro grains) creates strain and thus main lattice defect occurs, which decreases with further increase in temperature. The X-ray density is estimated by using the formula,

$$\rho_x = 8M/N\ a^3 \qquad (3.6)$$

Where a, N and M are lattice constant, Avogadro's number and molecular weight respectively. The values obtained are 6.75, 6.72 and 6.66 g/cm$^3$ respectively. The values of dislocation density (equation 3.7) are also calculated

$$\rho = 1/ \langle D_{W\text{-}H} \rangle^2 \qquad (3.7)$$

corresponding to particle size calculated by Williamson-Hall plot method and are also presented in table 3.1.

**Table 3.1: Presenting size, strain, lattice constant, X-ray density, dislocation density values $CoFe_2O_4$: $SiO_2$ nanocomposites at different annealing temperatures**.

| **Temp. & time (2h)** | **Crystallite size $D_{D\text{-}S}$ (nm)** | **Crystallite size $D_{W\text{-}H}$ (nm)** | **Strain ε** | **Lattice constant (Å)** | **Dislocation density ($m^{-2}$)** |
|---|---|---|---|---|---|
| **250 °C** | 19.80 | 20.26 | 1.01 x$10^{-2}$ | 8.032 | 2.43 x $10^{15}$ |
| **500 °C** | 27.15 | 28.95 | 2.72 x$10^{-3}$ | 8.062 | 1.19 x $10^{15}$ |
| **750 °C** | 35.34 | 38.76 | 3.75 x$10^{-3}$ | 8.069 | 6.66 x $10^{14}$ |

### 3.3.2 Fourier Transform Infrared (FTIR) Analysis

The Fourier transform infrared spectra of different samples like (a) as-prepared and those annealed at (b) 250 °C (c) 500 °C and (d) 750 °C for 2 h in frequency range of 4000-400 cm$^{-1}$ is exposed in the figure 3.5. In common, the infrared transmission spectra of the studied samples provide significant knowledge about the structural transformation, composition of phase and bonding among the ions in the samples. The spectra of as prepared sample of $CoFe_2O_4$: $SiO_2$ nanocomposite indicates

presence of bands at 3398.5 $cm^{-1}$ and 3404$cm^{-1}$ which are assigned to the stretching reflections of water (H-O-H) and surface silanol group (Si-OH) respectively [46]. This spectrum confirms the water band overlaps with the surface hydroxyl band vibrations thus making the band broad. Obviously, there are surely some quantity of microspores that exist in the present sample. These pores hold absorbed water. Further the intense absorptions at 1095.57, 798.53 and 464.84 $cm^{-1}$ point towards the configuration of silica network [47-49]. While the group seen at 578.69 $cm^{-1}$ is indication of Si–O–Fe group. The presence of Si–O–Fe vibrations reflects some chemistry connecting the isolated $Fe^{3+}$ ions and the nearest silica matrix. The appearance of Si–O–Fe and Co–O bonds adequately reflects the chemical character of the transition metals mixed up in the nanocomposites. These transition metal ions do not contribute straight in the sol–gel chemistry also when they were present into the precursor solutions as soluble inorganic salts [50]. From the spectra, it can be observed that band there at 1650 $cm^{-1}$ indicate the deformation of molecular water [38]. We can experience in the as-prepared and 250 $^0$C spectra, that band situated at 1650 $cm^{-1}$ has a strong affinity to these samples. The existence of this band yet at high temperature of 500 $^0$C and 750 $^0$C concludes that water molecules are still there in the structural conformation also seen from respective spectra. For the samples thermally treated at temperature of 500 $^0$C, the absorption band seen at 1095.57 $cm^{-1}$ for Si–O–S is of the $SiO_4$ tetrahedron is broadened further, while that for O–Si–O symmetric bond stretching vibrations at 464.84 $cm^{-1}$ and vibrational mode of Si-O-Si bond present at 800 $cm^{-1}$ become much weaker, which corresponds to a rescheduling process of silica network [51]. Appearance of broad hump at 3425 $cm^{-1}$ indicates Si-OH vibrations. Correspondingly, band centred around 578 $cm^{-1}$ show that the absorption of the Fe–O stretching in Fe–O–Si bond is intensified. These facts reflect the formation of $CoFe_2O_4$ composite with the rearrangement of silica network. Furthermore for the samples heat treated at 750 $^0$C, the IR spectrum changes significantly as compared with that for samples heat treated at lower temperatures. The band at 1095$cm^{-1}$ is coupled with the transversal optical (TO) mode of the Si-O-Si asymmetric stretching reflection. The reflection at 1095 $cm^{-1}$ for Si–O–Si of the $SiO_4$ tetrahedron grows slender and stronger, while the band at 956 $cm^{-1}$ was vanished [52-57]. The poor development of ferrite structure in as-prepared sample is evidenced by the weakening of characteristic band of ferrite (578 $cm^{-1}$). This fact is in agreement with XRD results, which

showed poor crystallinity in the as-prepared sample. Moreover, at high temperature, elimination of water molecule and Si-OH volatiles from the sample leads to densification of $CoFe_2O_4$:$SiO_2$ justifying the formation of nanocomposites which is confirmed by XRD.

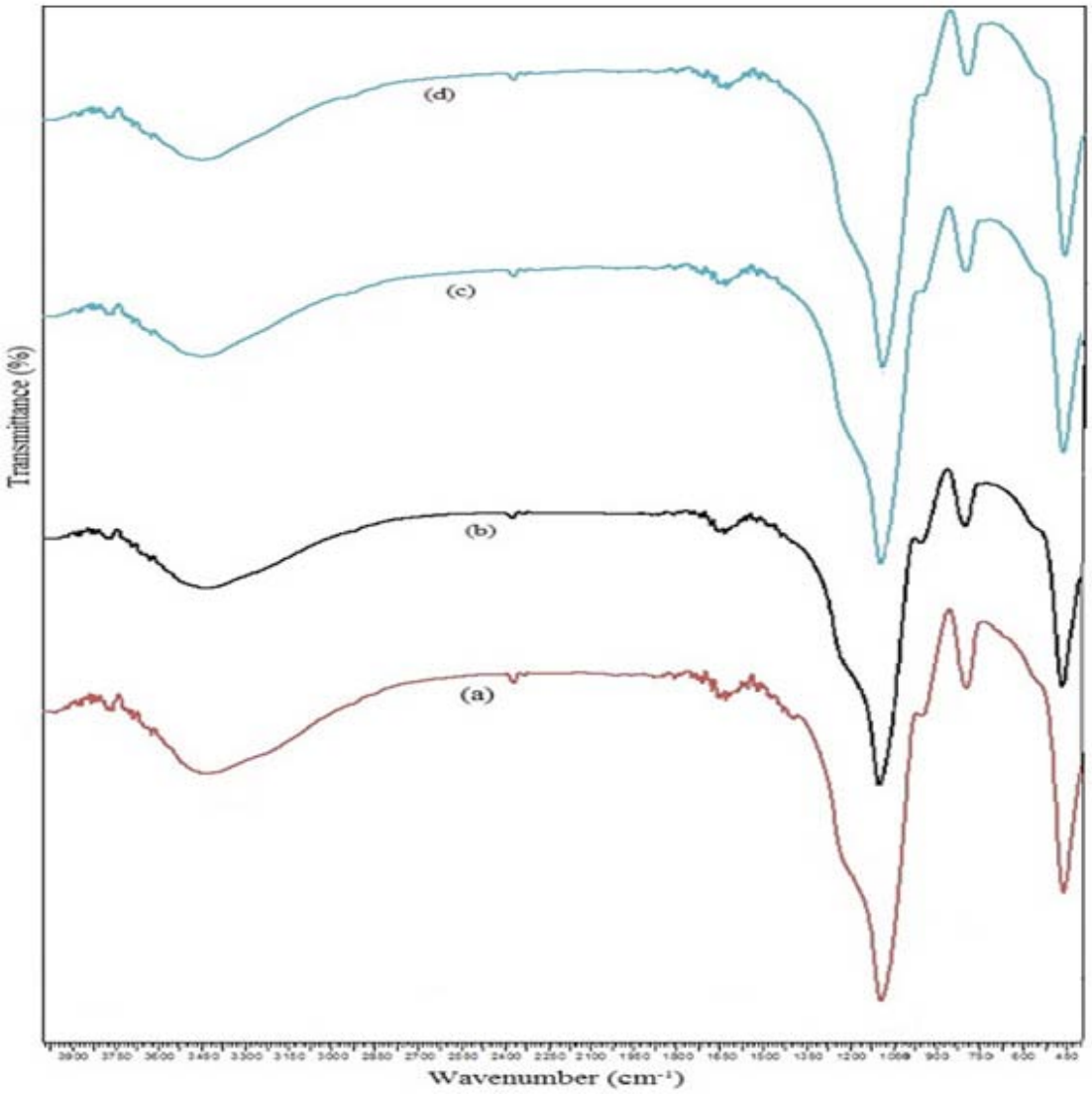


**Fig. 3.5: FTIR spectra of $CoFe_2O_4$:$SiO_2$ nanocomposites (a) as-prepared (b) $250^0$C (c) $500^0$C and (d) $750^0$C**

### 3.3.3 Scanning Electron Microscope (SEM) Analysis

The micrograph of $CoFe_2O_4$: $SiO_2$ nanocomposites are as shown in Figure 3.6. Figure 3.6(a) shows the micrograph of the samples thermally treated at 250 $^0$C. The SEM image shows agglomeration of nanoparticles at low temperature. Agglomerations signifies that particles do not show any well defined shape and also from XRD results, the sample synthesized at low temperature do not possess well developed

nanocomposites and crystallinity is poor. Poor crystallinity is a consequence of agglomeration. Also silica being amorphous in nature, show dominating behaviour at low temperature and thus this adds to poor crystallinity of samples... However a non uniform morphology of grown $CoFe_2O_4$ nanoparticles has already been reported [57]. The micrographs of $CoFe_2O_4$: $SiO_2$ nanocomposites thermally treated at 500 $^0$C and 750 $^0$C are shown in Figures 3.6(b) and 3.6(c). The micrograph of sample heat treated at 500 $^o$C shows feeble crystallinity and not very well developed nanoparticles. As discussed in XRD study that good crystallization of $CoFe_2O_4$: $SiO_2$ nanocomposites initiates at higher temperatures. The SEM picture of nanocomposites at 750 $^o$C distinctly exhibit narrow grain size distribution and presence of sphericity. As the process of re-crystallization speed up at this temperature and better crystallinity is achieved. The magnetic inter-particles and Vander Waal's interactions are dominant at low temperature (250 $^0$C) as compared to that at high temperature (500 $^o$C) and (750 $^o$C).

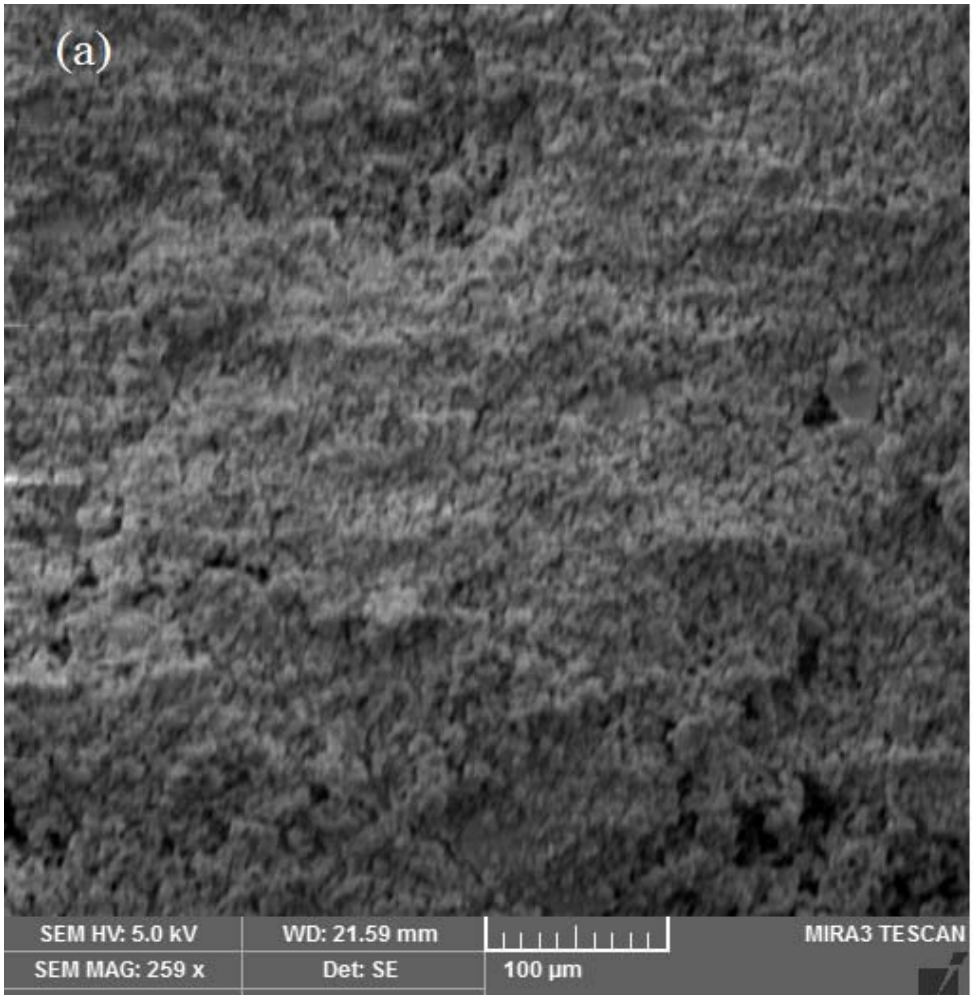


**Fig. 3.6: (a) SEM micrograph of $CoFe_2O_4$:$SiO_2$ nanocomposites at 250 $^o$C**

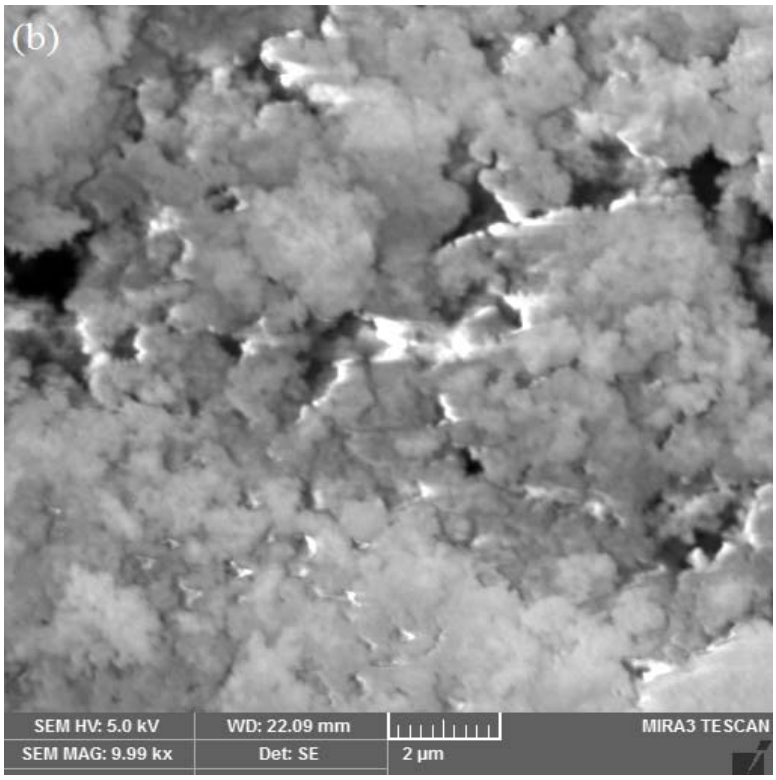


**Fig. 3.6: (b) SEM micrograph of $CoFe_2O_4$:$SiO_2$ nanocomposites at 500 $^oC$**

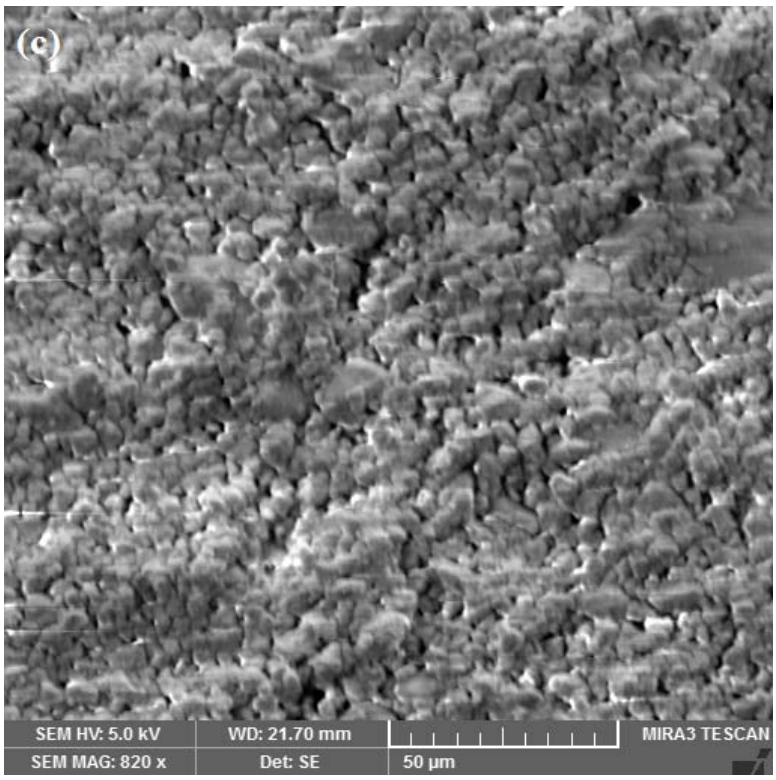


**Fig. 3.6: (c) SEM micrograph of $CoFe_2O_4$:$SiO_2$ nanocomposites at 750 $^oC$**

The appearance of agglomerates of both the SEM images indicates that there is decrease in the agglomeration of particles at higher temperature as compared to that at lower temperature. Hence the result indicates that individual appearance of the particles has enhanced at higher temperature.

### 3.3.4 Transmission Electron Microscope (TEM) Analysis

The morphology of the samples of $CoFe_2O_4$: $SiO_2$ nanocomposites annealed at 750$^o$C and 1000$^o$C for 2 hrs has been analysed by Transmission electron microscope (TEM-TECNAI 200kV) measurements. Carbon Coated copper grid was used to place a thin layer of sample for the analysis of nanocomposites. Figure 3.7 (a) represent TEM micrograph of $CoFe_2O_4$: $SiO_2$ nanocomposites annealed at 750$^o$C (b) represents micrograph of $CoFe_2O_4$: $SiO_2$ nanocomposites annealed at 1000$^o$C

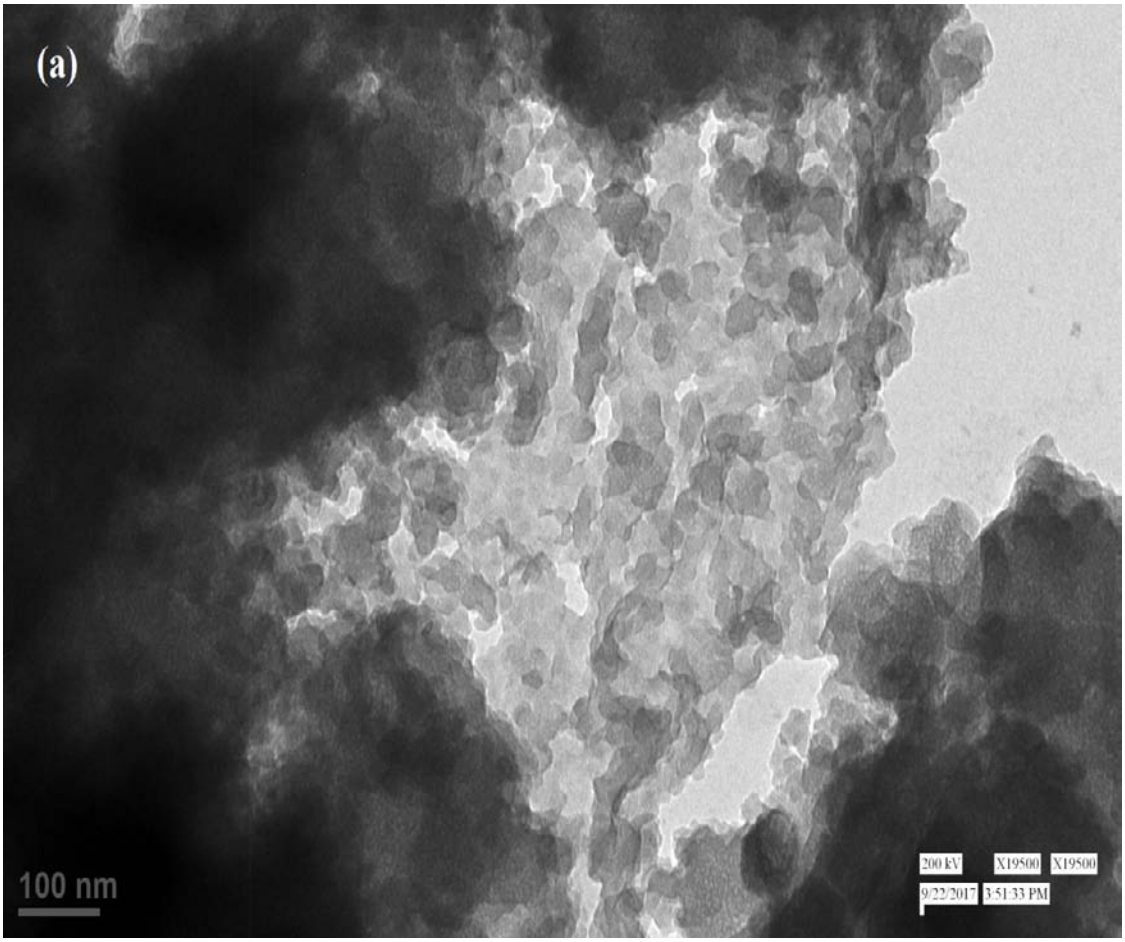


**Fig. 3.7: (a) TEM micrograph of $CoFe_2O_4$:$SiO_2$ nanocomposites annealed at 750$^o$C**

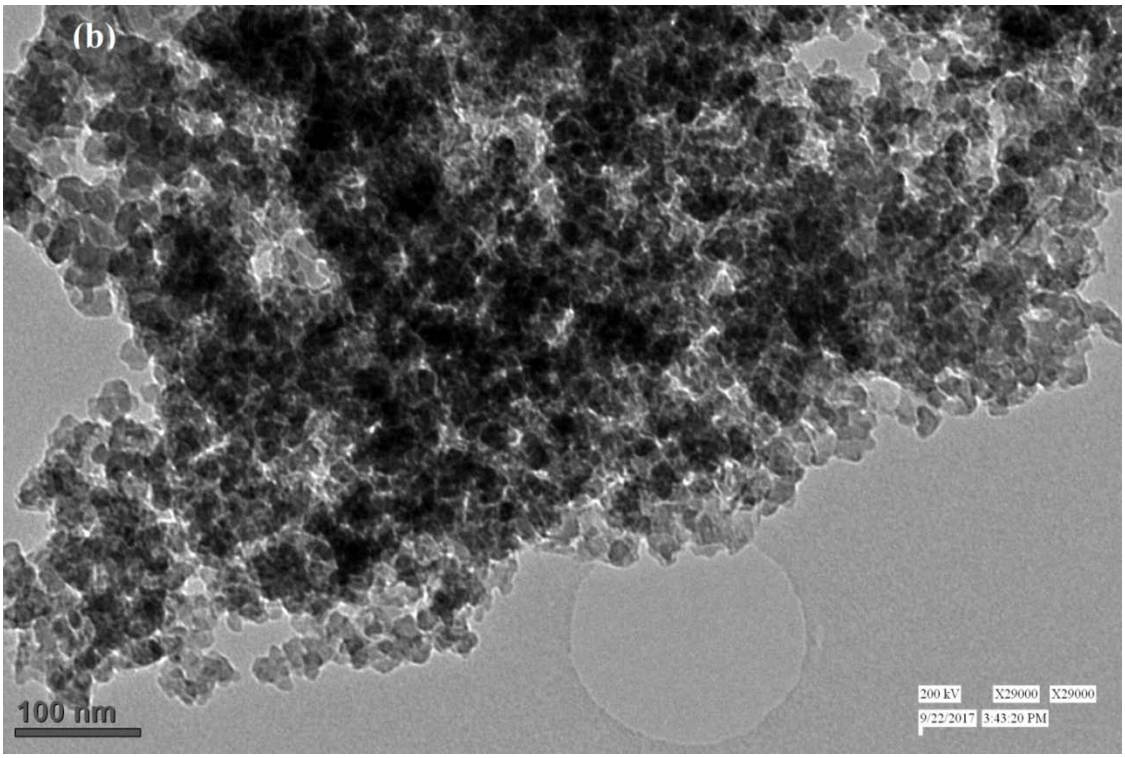


**Fig. 3.7: (b) TEM micrograph of $CoFe_2O_4$:$SiO_2$ nanocomposites annealed at 1000$^o$C**

In figure 3.7(a), the $CoFe_2O_4$:$SiO_2$ nanocomposites display spherical shaped nanoparticles and presence of aggregation. The average crystallite size is calculated and observed to be about 35nm. TEM results show resemblance with XRD results. TEM micrographs are preferred at 750$^o$C and higher temperature because at lower temperature, no well dispersed and well defined nanoparticles are obtained. The aggregated particles tend to produce bigger particles. The TEM picture of sample (Fig. 3.7 b) at 1000 $^o$C displays much better sphericity and particle size found to be about 38nm. It may be mentioned from resemblance of TEM results with XRD for particle size and then sharpness of XRD peaks that recorded micrographs indicate good quality samples and appearing approximate spherical shape $CoFe_2O_4$ nanoparticles with silica [58].

Histogram in figure 3.8 (a) and (b) represents the particle distribution corresponding to particle size range for the sample heat treated at 750 $^o$C and 1000 $^o$C. Histograms reveal an important information that nearly 75% of crystallites are having their size range of 30-42 nm representing a wide grain size distribution of crystallites. On observing histograms, it is seen that out of this 75% distribution, 60% of particles are distributed in grain range of 36-40 nm.

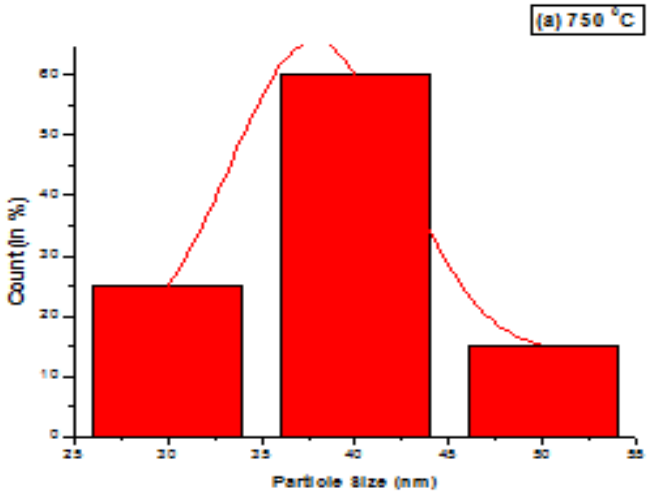


**Fig. 3.8: (a) Histogram of $CoFe_2O_4$:$SiO_2$ nanocomposites annealed at 750°C**

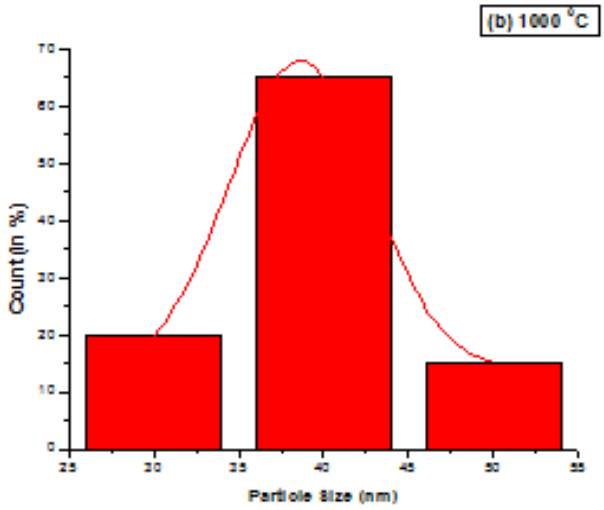


**Fig. 3.8: (b) Histogram of $CoFe_2O_4$:$SiO_2$ nanocomposites annealed at 1000°C**

### 3.3.5 Thermogravametric (TGA-DTG) Analysis

The thermal decomposition behaviour of precursors was investigated by themogravametric (TGA- DTG) analysis. TGA-DTG curves of the powdered $CoFe_2O_4$:$SiO_2$ nanocomposites sample is shown in Fig. 3.9. Thermogravametric examination of precursors revealed that a total weight loss of 24% occurred when the complete temperature range is divided into four different temperature ranges as 50°C -200°C, 201°C - 350°C, 351°C – 600°C, 601°C -750°C. When the powdered sample was heated from 50°C to 200°C (first stage), around 7.0% weight loss occurred due to the loss of moisture of water from the sample. This loss of moisture

is also reflected in the DTG curve by the presence of peak at $114^0$C. In the second stage ($201^o$C -$350^0$C) nearly 11% weight loss was observed. This weight loss might be due to the oxidative decomposition of precursors. Presence of a strong peak at temperature around $208^o$C attributes to the decomposition of precursors in the DTG curve [59].In the third stage (351 $^o$C - $600^0$C), a constant weight loss is observed leading to the formation of an intermediate structure of $CoFe_2O_4$:$SiO_2$. In the temperature range $601^o$C -$750^o$C, the negligible weight loss implying strengthening of intermediate structure of $CoFe_2O_4$:$SiO_2$ nanocomposites. No weight loss was observed when the sample was further heated beyond $750^o$C. This confirmed the full decomposition of precursors and formation of stable structure of the $CoFe_2O_4$:$SiO_2$ nanocomposites.

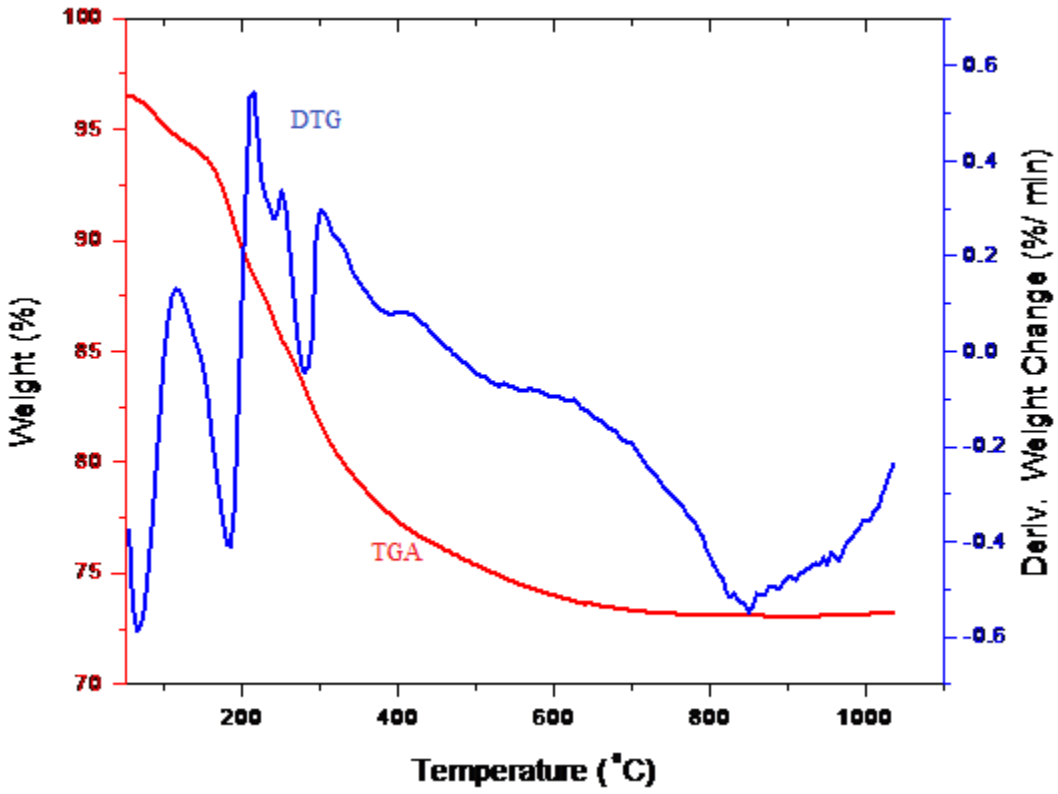


**Fig. 3.9: TGA-DTG curve of $CoFe_2O_4$:$SiO_2$ nanocomposites**

However, on clearly analysing DTG curve of $CoFe_2O_4$:$SiO_2$ nanocomposites, strong peak appeared at temperature 217°C indicates the decomposition process. This decomposition corresponds to that of water molecules in the form of moisture and residual nitrates. No additional knowledge about the symmetry, phase and type of structure is provided by TGA analysis even at high temperatures. From the TGA

curve, stabilization of structure is visualized at and after 700 $^oC$, that is stable formation of nanocrystallites at this temperature called re-crystallization temperature) is achieved. This is also favoured by XRD results.

### 3.3.6 Vibrating Sample Magnetometer (VSM) Analysis

The M-H curves of samples observed at three different values of temperatures are shown in the fig3.10.The variations in important magnetic parameters like saturation magnetisation (Ms), residual magnetization (Mr) and coercivity (Hc) as a function of temperature have been listed in the Table 3.2. These consequences indicate that above mentioned all these magnetic properties of $CoFe_2O_4$:$SiO_2$ nanocomposites show highly reliance behaviour upon the annealing temperatures. The value of Ms enhances from 53.6 ±0.1 emu/g to 55.3±0.1 emu/g and from 55.3±0.1emu/g to 63.7±0.1emu /g with the raise of temperature from 250$^oC$ and 500$^oC$ and again from 500$^oC$ to 1000$^oC$ respectively. However, the value estimated for saturation magnetization of silica dispersed cobalt-ferrite nanocrystallites when compared with their bulk value of 80.8emu/g was detected to have smaller value [53]. This difference in value of saturation magnetization for two different states of $CoFe_2O_4$:$SiO_2$ could be elucidated with the description of core- shell model, that describe about the finite size effects of nanoparticles that merge from the spin tilting effect in ferromagnetism or non-colinearity of spins and consequently magnetization reduces[38]. A similar kind of behaviour progression also observed for residual magnetization (Mr) changes value from 15.48 emu g−1 on 250$^oC$ towards 21.48 emu $g^{-1}$ on 500$^oC$. But when samples are heat treated at 1000$^oC$ a decrease in Mr is observed leading to surface canting effects as seen from the Table 3.2. It can be deduced from the progression behaviours of saturation value of magnetization (Ms) and residual magnetization (Mr) that are greatly dependent upon the development of $CoFe_2O_4$:$SiO_2$ nanosize crystallites. Moreover with raising the annealing temperature from 250$^oC$ toward 500$^oC$ an addition to in the values of magnetic parameters namely saturation and remnant magnetizations and average particle size has been observed, as seen from table3.1. Thus, modification in magnetic properties of cobalt-ferrite has been attributed as a consequence of variation of particle size as a function of temperature. From the results listed in table3.2, it may be noticed from discrepancy of Hc value that its behaviour is different as compared to Ms and Mr values which indicates that size of nanocrystallites is not the only aspect in deciding Hc values. It has been concluded by many other researchers that variations in the values of

Hc associated with different factors like microstructure, particle dimension and residual strain force [60-61]. The coercivity (Hc) varied from 2363Oe to 2181Oe with temperature from 500°C to 1000°C. The coercivity for pure CoFe2O4 nanoparticles is reported to be lower (980 Oe) as compared to $CoFe_2O_4/SiO_2$ nanoparticles [62]. This large divergence of $SiO_2$ dispersed cobalt ferrite from pure cobalt ferrite may be attributed to the presence of silica matrix that diversely affects the surface feature.

**Table 3.2: Magnetic parameters of $CoFe_2O_4$:$SiO_2$ nanocomposites**

| Temperature (°C) | Ms (emu/g) | Mr (emu/g) | Hc (Oe) | R=Mr/Ms |
|---|---|---|---|---|
| 250 °C | 53.6±0.1 | 15.48 | 2363 | 0.29 |
| 500 °C | 55.3±0.1 | 21.48 | 2363 | 0.39 |
| 1000 °C | 63.7±0.1 | 19.79 | 2181 | 0.31 |

From the Table 3.2, values of remnant ratio R=Mr/Ms indicate that direction of magnetization that easily reorients to its nearest axis direction after removal of magnetic field.

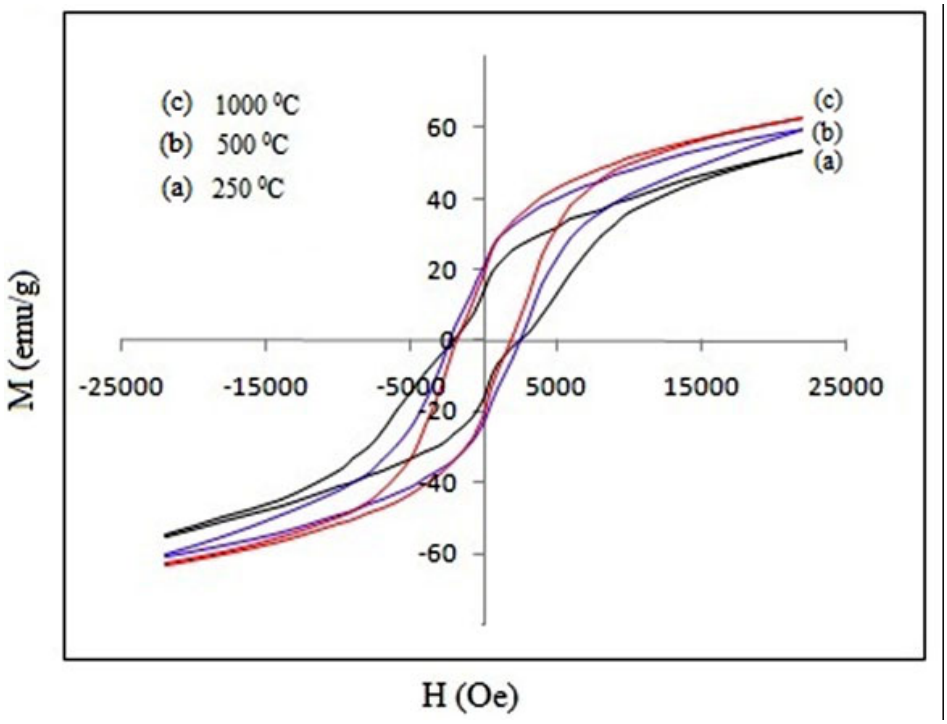


**Fig. 3.10: Hysteresis loop of $CoFe_2O_4$:$SiO_2$ nanocomposites annealed at different temperatures**

### 3.4 Conclusions

$CoFe_2O_4$:$SiO_2$ nanocomposites were prepared successfully by wet chemical route owning to coprecipitation method. After the preparation of $CoFe_2O_4$:$SiO_2$ powder sample, subsequent heat treatment at 250 $^oC$, 500 $^oC$, 750 $^oC$ and1000 $^oC$ for 2hrs was carried out. pH value 12 was maintained to achieve better precipitation. XRD results exposed that crystallization of silica dispersed cobalt ferrite is achieved at comparatively high temperature of 750 $^oC$ . Desirable samples of silica embedded cobalt-ferrite nanocomposites were confirmed on the basis of their characterization results. With the help of XRD data, the lattice constant has been found to increase from 8.032 Å to 8.069 Å by increasing the calcinations temperature from 250°C to 750°C respectively. Presence of silica was confirmed by a broad hump appeared at 2θ positioned around 21-25$^o$ in all the XRD pictures. Particle sizes for the synthesized samples were examined by Debye- Scherrer equation and also by Williamson- Hall method that includes the effects of stress/strain. The particle size is reported by W-H method 20.26 nm, 28.75 nm and 38.76nm at temperatures 250 $^oC$, 500 $^oC$ and 750 $^oC$ respectively, supported by TEM results.TEM investigation conclude aggregation of particles leading to an increase in particle size. Nearly about 75% of crystallites are having the size range 30-42 nm at 750 $^o$ from TEM investigations, indicates a wide grain size distribution of crystallites. Also spherical behaviour of nanoparticles was seen from TEM analysis of samples at 750$^o$C and 1000$^o$C. Results of our research concluded that there is an increase in particle size, crystallinity, surface morphology and microstructure of nanocomposites with increasing calcinations temperature.

FTIR spectra provide significant knowledge about the structural transformation, composition of phase and bonding among the ions in the samples. The spectra of as prepared sample of $CoFe_2O_4$: $SiO_2$ nanocomposite confirms the presence of water (H-O-H) and surface silanol group (Si-OH) bands at 3398.5 $cm^{-1}$ and 3404$cm^{-1}$. The IR spectrum changes significantly at 750 $^oC$ as compared with that for samples heat treated at lower temperatures. The poor development of ferrite structure in as-prepared in agreement with XRD results. At high temperature, elimination of water molecule and Si-OH volatiles from the sample leads to densification of $CoFe_2O_4$:$SiO_2$ justifying the formation of nanocomposites which is confirmed by XRD.

SEM study analyzes the morphology of nanocomposites. The SEM image shows agglomeration of nanoparticles at 250 $^oC$, Whereas better sphericity of nanocomposites was noticed at high temperature of 750 $^oC$.

Effect of heat treatment on precursor's decomposition and development to a stable structure was concluded from TGA analysis. A weight loss of 24% was observed throughout the process. At high temperature negligible weight loss indicates about formation of stable structure. From DTG curve, appearance of strong peak at temperature 217°C indicates the decomposition of water molecules in the form of moisture and also of residual nitrates.

Further, the value of saturation magnetization ($M_s$) is reported 53.6±0.1 emu/g and 63.7±0.1 emu/g corresponding to the calcinations temperature 250°C and 1000°C respectively. On the basis of VSM results at room temperature, it can be concluded that magnetic properties such as retentivity, saturation magnetization and coercivity revealed a strong dependence on the crystallite size and calcinations temperature. Furthermore, non-uniform behaviour of residual magnetization may be related to surface canting or spin's non-colinearity in our synthesized nanocomposites.

**References**

[1]. Mnyusiwalla, A.; Daar, A.S.; Singer, P.A. Mind the gap: science and ethics in nanotechnology, Nanotechnology., 14 (2003), R9.

[2]. Buot, F.A. Mesoscopic physics and nanoelectronics: nanoscience and nanotechnology, Physics Reports., 234(1993) , 73-174.

[3]. A.B. Gadkari, T.J. Shinde, P.N. Vasambekar, Mater.Chem. Phys. 114(2009) 505.

[4]. L. Gama, A.P. Diniz, A.C.F.M. Costa, S.M. Bezende, A. Azevedo, D.R. Cornejo, Physica B: Conden. Matter. 384(2006) 97.

[5]. S.E. Jcoba, S. Dukalde, H.R. bertorella, J. Magn. Magn. Mater. 2253(2004) 272Pardavi-Horvath, M. J. of Magn and Magn Mater., 215(2000**)**, 171-183.

[6]. N. Rezlescu, E, Rezlescu, F. Tudorach, P.D. Popa, J. Opt. Adv. Mater. 6(2004) 695.

[7]. X. Chu, B. Cheng, J. Hu, H. Qin, M. Jiang, Sensors. Actuat. B 129(2008) 53.

[8]. K. Raj, R. Moskowitz, R. Casciari, J. Magn. Magn. Mater. 149(1995) 174.

[9]. E. Melagiriyappa, H.S. Jayanna, J. Alloys and Comps. 482(2009) 147.

[10]. N.A. Spaldin, M. Fiebig, The renaissance of magnetoelectric multiferroics, Science (New York, NY) 309(2005) 391.

[11]. J. Smit and H. P. J. Wijn Ferrites (Philips Technical Library, Eindhoven, (1959).

[12]. Pardavi-Horvath, M. J. of Magn and Magn Mater., 215(2000**)**, 171-183.

[13]. Huang, X.H.; Chen, Z.H. Solid State Commun., 132(2004**)**, 845–850.

[14]. Jung, J.S.; Lim, J.H.; Choi, K.H.; Oh, S.L.; Kim, Y.R.; Lee, S.H.; Smith, D.A.; Stokes, K.L.; Maljinski, L.; Oconnor, C.J. J. Appl. Phys., 97(2005**)**, 10F306.

[15]. Virden, A.E.; Ogrady, K. J. Appl. Phys., 99(2006**)**, 08S106.

[16]. Srinivasan, S. Y., Paknikar, K. M., Bodas, D., and Gajbhiye, V., Applications of cobalt ferrite nanoparticles in biomedical nanotechnology. Nanomedicine, 13(10) (2018), 1221–1238. doi:10.2217/nnm-2017-0379

[17]. Harris, V.G.; Chen, Z.H.; Chen, Y.J.; Yoon, S.; Sakai, T.; Gieler, A.; Yang, A.; He, Y.X.; Ziemer, K.S.; Sun, N.X.; Vittoria, C. J. Appl. Phys., 99 (2006), 08M911.

[18]. Jyotsnendu, G.; Theerdhala, S.; Saket, A.; Tumkur, G.R.; Arun, K.N.; Dhirendra, K.B. J. Magn. Magn. Mater., 293 (2005), 55.

[19]. H. St. C. O'neill, M. james, Wayne, Dollase, Simon and T. Redfern, Temperature dependence of the cation distribution in $CuAl_2O_4$ spinel, Eur. J. Mineral. 17 (2005) 581-586.

[20]. Cullity, B.D. Elements of X-ray Diffraction, Addison-Wesley Reading MA., (1959).

[21]. Valenzuela, R. (1994). Magnetic Ceramics. Cambridge, Cambridge University Press, 10.1017/CBO9780511600296.

[22]. Coey, J. M., Magnetism in future. Journal of Magnetism and Magnetic Materials., 226-230(2001), 2107-2112.

[23]. Kingery, W. D., Bowen, H. K., & Uhlmann, D. R., Introduction to Ceramics 2. ed. New York, John Wiley & Sons, (1976).

[24]. Silva, J. B., Brito, W. ., & Mohallem, N. D. S., Influence of the heat treatment on cobalt ferrite nanocrystal powders. Materials Science and Engineering. B, Solid State Materials for Advanced Technology, 112(2004), 182-187.

[25]. Hench, L. L., & West, J. K., Principles of Electronic Ceramics.Wiley, (1990).

[26]. Grigorova, M., Blythe, H. J., & Blaskov, V., Magnetic properties and Mössbauer spectra of nanosized $CoFe_2O_4$ powders. J. Magnet. Magnet. Mat, 183(1998), 163-172.

[27]. Qu, Y., et al., The effect of reaction temperature on the particle size, structure and magnetic properties of coprecipitated $CoFe_2O_4$ nanoparticles. Mater. Lett, 60(2006), 3548-3552.

[28]. Song, Q., & Zhang, Z. J., Correlation between spin-orbital coupling and the superparamagnetic properties in magnetite and cobalt ferrite spinel nanocrystals. J. Phys. Chem. B. V. 110, 23(2006), 11205-11209.

[29]. Huang, X.; Chen, Z. J. Magn Magn Mater., 280(2004), 37–43.

[30]. Chien, C.L.; Annu.Rev. Mater. Sci., 25(1995**)**,129.

[31]. Sutka, A.; Mezinskis, G.Frontiers of Materials Science., 6(2012**)**, 128-141.

[32]. Mathew, D.S.; Juang, R.S. Chemical Engineering Journal., 129(2007), 51-65.

[33]. Liu, C.; Zou, B.; Rondinone, A.J.; Zhang, Z. J. J. Am. Chem. Soc., 122(2000**)**, 62-63.

[34]. Pillai, V.; Shah, D.O. J. Magn. Magn. Mater., 163(1996), 243.

[35]. Lee, J.G.; Park, J.Y. ; Kim, C.S.J. Mater. Sci. 33(1998), 396.

[36]. Yeong, K.I.; Don, K.; Choong, L.S. Physica B., 337 (2003), 42.

[37]. Morais, P.C.; Garg, V.K.; Oliveira, A.C. ; Silva, L.P.; Azevedo, R.B.; Silva, A.M.L.; Lima, E. C.D. J. Magn. Magn. Mater., 225(2001), 37.

[38]. S. Xavier, S. Thankachan, B. P.Jacob, E.M. Mohammed, Nanosystems: Phys.Chem. Math., 4 (2013) 430-437.

[39]. S. Duhan, P. Aghamkar, N. Kishore , B. Lal, Materials Chemistry and Physics, 114 (2009) 103-106.

[40]. C. Thiriet-Dodane, Study of irradiation damages in $MgAl_2O_4$ and $ZnAl_2O_4$ spinels in the framework of nuclear waste transmutation, Report CEA-R-6010-Comunissariat ´al' Energie Atomique France (2002).

[41]. M.J. Buergers, Crystal Structure Analysis, Wily, New York/ London (1960).

[42]. D .Y. Li and B. H. O' connor, Advances in X-ray Analysis, Plenum Press, New York, (1992).

[43]. H. St. C. O'Neill and W. A. Dollase, Crystal Structures and Cation Distributions in Simple Spinels from Powder XRD Structural Refinements: $MgCr_2O_4$, $ZnCr_2O_4$, $Fe_3O_4$ and the Temperature Dependence of the Cation Distribution in $ZnAl_2O_4$, Phys. Chem. Minerals 20 (1994) 541-555.

[44]. D. Simeone, C. Dodane-Thiriet, D. Gosset, P. Daniel and M. Beauvy, Order–disorder phase transition induced by swift ions in $MgAl_2O_4$ and $ZnAl_2O_4$ spinels, J. Nucl. Mater. 300 (2002) 151-160.

[45]. T.J. Shinde, A.B. Gadkari, P.N. Vasambekar, J. Mater. Sci. Mater. Electron. 21 (2010) 120-124.

[46]. Dippong, T., Levei, E. A., & Cadar, O. (2017). Preparation of $CoFe_2O_4$/$SiO_2$ Nanocomposites at Low Temperatures Using Short Chain Diols. Journal of Chemistry, (2017) 1–11. doi:10.1155/2017/7943164

[47]. P.D. Maniar, A. Navrotsky, E.M. Rabinovich, J.Y. Ying, J.B. Benziger, J. Non-Cryst. Solids 124 (1990) 101–111.

[48]. I.K. Battisha, Indian J. Pure Appl. Phys. 40 (2002) 122–131.

[49]. H. Ono, T. Katsumata, Appl. Phys. Lett. 78 (2001) 1832–1834.

[50]. L.A. Garcia Cerda, S.M.Montemayor, J. Magn.Magn. Mater. 294 (2005) e43–e46.

[51]. J.M.D. Coey, Phys. Rev. Lett. 27 (1971) 1140–1142.

[52]. X.H. Huang, Z.H. Chen, Scripta Materialia 54 (2006) 169–173.

[53]. S.H. Xiao, H.J. Xu, J. Huc, L.Y. Li, X.J. Li, Physica E 40 (2008) 3064–3067.

[54]. S.R. Mekala, J. Ding, J. Alloys Compd. 296 (2000) 152–156.

[55]. S. Zhang, D. Dong, Y. Sui., Z. Liu, H. Wang, Z. Qian, W. Su, J. Alloys Compd. 415 (2006) 257–260.

[56]. J.B. Silva, C.F. Diniz, R.M. Lago, N.D.S. Mohallem, J. Non-Cryst. Solids 348 (2004) 201–204.

[57]. A. Raval, N. Panchal, R. Jotania, International Journal of Modern Physics, 22 (2013) 558–563.

[58]. Xianghui, H.; Zhenhua; C. Chinese Sci Bull., 51(2006), 2529-2534.

[59]. A.B. Rajput , S. Hazra, N.N. Ghosh, J. Exp. Nanosci, , 8:4(2013), 629-639.

[60]. Liu, B.H.; Ding, J. Appl. Phys. Lett., 88(2006**)**, 042506-1.

[61]. Wang, Y.C.; Ding, J.; Yi, J.B.; Liu, B.H.; Yu, T.; Shen, Z.X. Appl. Phys. Lett., 84(2004), 2596-2598.

[62]. Xiao, S. H.; Jiang, W. F.; Lia, L. Y.; Li, X. J. Mater. Chem. Phys., 106(2007), 82–87.